ACS OMEGA

http://pubs.acs.org/journal/acsodf

Article

Structural Characterization of Polycrystalline Titania Nanoparticles on *C. striata* Biosilica for Photocatalytic POME Degradation

Rindia M. Putri,* Novi Syahra Almunadya, Aryan Fathoni Amri, Nadia Tuada Afnan, Zeily Nurachman, Hary Devianto, and Wibawa Hendra Saputera*

Cite This: *ACS Omega* 2022, 7, 44047−44056

Read Online

ACCESS | Metrics & More | Article Recommendations | Supporting Information

ABSTRACT: The biosilica shell of marine diatoms has emerged as a unique matrix for photocatalysis, owing to its sophisticated architecture with hierarchical nanopores and large surface area. Although the deposition of titania nanoparticles on diatom biosilica has been demonstrated previously, their photocatalytic activity has been tested only for degradation of pure compounds, such as dyes, nitrogen oxide, and aldehydes. The efficiency of such photocatalysts for degradation of mixtures, for instance, industrial wastewaters, is yet to be investigated. Furthermore, reports on the lattice structures and orientation of nanotitania crystals on biosilica are considerably limited, especially for the underexplored tropical marine diatoms. Here, we report an extensive characterization of titania-loaded biosilica from the tropical *Cyclotella striata* diatom, starting from freshly grown cell cultures to photodegradation of wastewaters, namely, the palm oil mill effluent (POME). As Indonesia is the largest palm oil producer in the world, photocatalytic technology could serve as a sustainable alternative for local treatment of POME. In this study, we achieved a 54% loading of titania on *C. striata* TBI strain biosilica, as corroborated by XRF analyses, which was considerably high compared to previous studies. Through visualization using HR-TEM, supported by SAED and XRD analyses, nanocrystal TiO_2 appeared to be trapped in an anatase phase with polycrystalline characteristics and distinct crystallographic orientations. Importantly, the presence of *C. striata* biosilica lowered the band gap of titania from 3.41 eV to around 3.2 eV upon deposition, enabling photodegradation of POME using a broad-range xenon lamp as the light source, mimicking the sunlight. Kinetic analyses revealed that POME degradation using the photocatalysts followed quasi-first-order kinetics, in which the highest titania content resulted in the highest photocatalytic activity (*i.e.*, up to 47% decrease in chemical oxygen demand) and exhibited good photostability throughout the reaction cycles. Unraveling the structure and photoactivity of titania-biosilica catalysts allows transforming marine diatoms into functional materials for wastewater photodegradation.

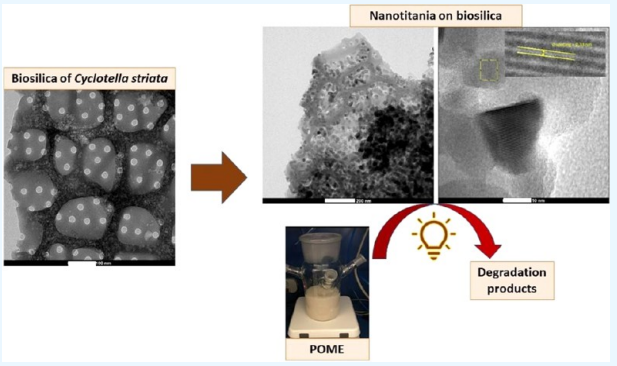

1. INTRODUCTION

Unlike most unicellular organisms with carbohydrate-based cell walls, single-celled diatoms are characterized by their porous silica shells, making them one of the most unique creatures inhabiting the ocean, including the tropical coastlines. The silica shells form a highly organized three-dimensional architecture with characteristic pores of hundreds of nanometers, which are inferred to be the gates for nutrition influx for cell growth. As photosynthetic microorganisms, diatoms supply up to a quarter of oxygen worldwide and greatly contribute to sustaining the marine ecosystem.[1] In recent years, diatoms have gained attention as abundant, sustainable, and inexpensive sources of biosilica.[2,3] Laboratory cultivation of diatoms has been studied and proven to maintain their sophisticated structures upon various treatments to obtain pure biosilica. In recent years, the biosilica of diatoms has been demonstrated as an effective matrix for catalysis, particularly photocatalysis.[4−9]

Among several photocatalysts, titania (TiO_2) has been frequently used due to its low-cost, nontoxic, and abundant nature.[10] However, TiO_2 possesses several disadvantages, such as poor stability, low absorption in the visible light region, and low adsorption of organic pollutants. Thus, modifications of the TiO_2 surface are required to overcome such issues. Deposition of titania particles on the biosilica porous surface was reported to stabilize the particles while providing higher adsorption of organic compounds and improving access to the active sites.[8,9] Several reports have investigated the photocatalytic efficiency of titania nanoparticles deposited on biosilica surfaces.[4−9]

Received: August 24, 2022
Accepted: November 4, 2022
Published: November 18, 2022

https://doi.org/10.1021/acsomega.2c05450
ACS Omega 2022, 7, 44047−44056

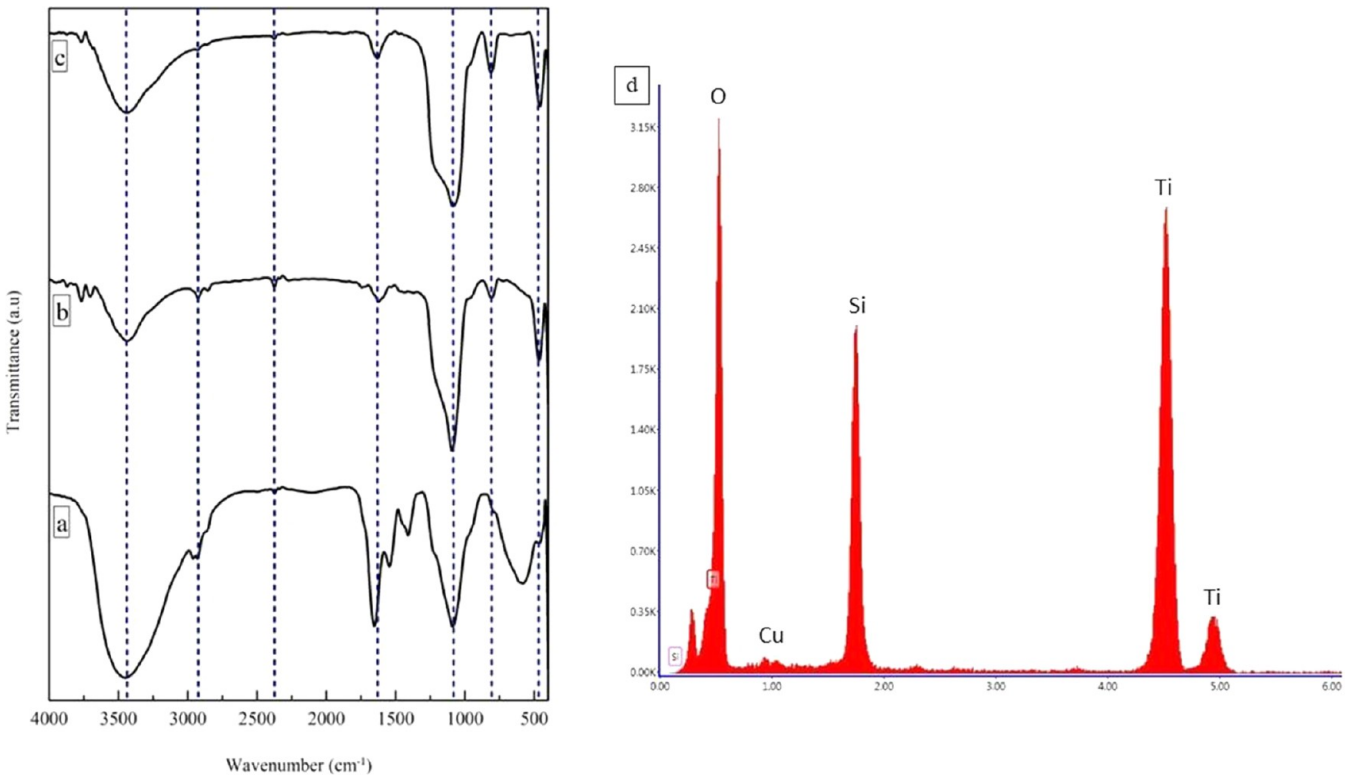

Figure 1. FT-IR spectra of (a) *C. striata* diatom biomass, (b) purified biosilica from diatom biomass, and (c) TiO_2-modified biosilica photocatalyst. (d) EDX spectrum of TiO_2-modified biosilica, showing the characteristic Ti bands.

However, previous studies have focused on the photodegradation of pure compounds, such as dyes,[4,7,11−15] antibiotic compounds,[16] nitrogen oxide,[9] and aldehydes.[6] Whether diatom-based photocatalysts could exhibit good performance for photodegradation of impure mixtures, as in wastewaters, is currently unknown. Furthermore, structural characterizations of titania-loaded biosilica (*i.e.*, crystallographic orientation and lattice visualization) are considerably limited, especially for the underexplored tropical marine diatoms, while structural differences could lead to different photocatalytic activities.

An example of wastewater that is regularly produced in a vast amount—for which photocatalytic treatment has been increasingly relevant—is the wastewater from palm oil plantations, namely, the palm oil mill effluent (POME).[17] Since almost 85% of palm oil circulating in the world is produced in Indonesia and Malaysia, it is important to develop a renewable and green photocatalytic technology to tackle the waste problem.[17] It is estimated that a ton of palm oil processing produces around 55−67% of POME, equivalent to more than 500 kg of POME.[17] The amount of POME rapidly skyrocketed over the years as Indonesia now produces more than 40 million tons of palm oil annually. As diatom-based photocatalysts hold great potential in reducing the environmental impact of POME, their catalytic capability should be evaluated.

In this report, we synthesize and characterize photocatalytic titania nanoparticles on the biosilica surface of *Cyclotella striata* TBI strain, a species of microalgae found abundantly on the Indonesian shore. We performed an extensive structural characterization on the particles, including HR-TEM, SAED, SEM, XRD, and EDX, as well as an examination of the band gap, to shed light on the origin of the photocatalytic activity. In addition, photocatalysis was specifically investigated for POME degradation to demonstrate that such systems are applicable to the photodegradation of wastewaters. To this end, developing modified biosilica from diatoms as a photocatalyst to process POME will serve as a means to transform renewable marine products into functional materials for environmental applications.

2. RESULTS AND DISCUSSION

The diatom used in this study, *C. striata* TBI strain, was sampled from the shore of Bidadari Island of Indonesia and cultivated in the lab using artificial saltwater as growth media. Previous studies have investigated the use of *Cyclotella* diatom as a template for biopolymerization,[18] antibiotic photodegradation,[16] and detection of biomolecules.[19] Meanwhile, the exploration of *Cyclotella* and other diatoms for photocatalysis of waste degradation, such as POME, has not been reported elsewhere. The cells of *C. striata* were brown in color and 10−20 μm in diameter. After two weeks of cultivation (Figure S1), laboratory-grown *C. striata* cells were processed into pure biosilica through oxidation and calcination (Figure S2 and Table S1).[20] On average, a gram of pure biosilica could be produced from 100 g of wet biomass.

To synthesize the photocatalysts, we used titanium(IV) oxysulfate as a precursor as it is nontoxic and environmentally friendly.[6] We modified the biosilica with titanium(IV) oxysulfate at a varying mole ratio of Ti/Si of 1:3, 1:2, 1:1, 2:1, and 3:1, respectively. We performed FT-IR analysis of the isolated biomass of *C. striata* diatom (Figure 1a), purified biosilica from biomass (Figure 1b), and TiO_2-modified biosilica (Figure 1c). Comparing biosilica to biomass (comparing panel b to panel a in Figure 1, respectively), it appeared that the organic contents of biomass were successfully removed during the treatment, as indicated by the disappearance of vibration bands of carbonyl, amines, and amides at 1250−1750 cm^{-1} in the biosilica

https://doi.org/10.1021/acsomega.2c05450
ACS Omega 2022, 7, 44047−44056

spectrum (Figure 1b). Oxidation of biomass using nitric acid, followed by drying and calcination, indeed resulted in a pure biosilica (Table S1), as characterized by the vibration bands of Si−O−Si at 462, 808, and 1087 cm^{-1} in Figure 1b. Meanwhile, Figure 1c shows that modification with TiO_2 did not alter the functional groups of biosilica, as the IR spectrum was identical to that of biosilica (Figure 1b). Rather than forming new covalent bonds, TiO_2 was likely immobilized by physisorption on the porous surface of biosilica, which is in agreement with previous reports.[4,13,21]

We further confirmed the presence of Ti using EDX (Figure 1d) and XRF (Table 1). Notably, the highest Ti content was achieved at a 2:1 initial ratio of Ti/Si, yielding a 54% TiO_2 in the TiO_2/SiO_2 composite (Table 1). Increasing the initial ratio of Ti/Si to 3:1 did not result in a higher Ti content in the composite, suggesting that the surface of the biosilica was already saturated with TiO_2 particles. Brunauer−Emmett−Teller (BET) isotherms for surface area analyses (Figure S3 and Table S2) also revealed that the photocatalyst with 54% TiO_2 (prepared from a 2:1 initial ratio of Ti/Si) had the lowest available surface area of around 22 m^2/g, compared to other variations of Ti/Si. A 54% loading of titania on pure biosilica is considerably high compared to a previous report, which peaked at around 29% (also based on XRF analyses).[6] The loading improvement might be attributed to nanoparticles coverage on the entire surface instead of concentrated inside the pores only.

Table 1. Ratio of TiO_2 and SiO_2 in the Photocatalysts Determined Using XRF

initial composition Ti:Si (mol)	%TiO_2	%SiO_2
1:3	8.53 ± 0.22	91.47 ± 0.19
1:2	27.66 ± 0.18	72.34 ± 0.33
1:1	41.19 ± 0.12	58.81 ± 0.30
2:1	53.79 ± 0.13	46.21 ± 0.44
3:1	48.77 ± 0.12	51.23 ± 0.35
biosilica only		100 ± 0.00

We further examined the morphology of TiO_2/biosilica in comparison to pure biosilica using SEM and HR-TEM. SEM images showed no major differences between the modified and non-modified biosilica (Figure 2). Both particles were circular, as centric diatoms in general, with visible porous surfaces. However, the SEM image of TiO_2/biosilica showed more disintegrated particles and opening of the pores (Figure 2b), possibly due to chemical and physical treatment during the synthesis (*e.g.*, oxidation and constant stirring). Interestingly, HR-TEM images of biosilica clearly showed the presence of hierarchical pores of *C. striata* diatom (Figure 3a), displaying both larger pores of 100−200 nm and several smaller pores (within the larger pores) of 3−10 nm each (Figure 3b). However, upon magnification at a 10 nm scale, no organized structure was observed for pure biosilica, indicating an amorphous form (Figure 3c).

Upon modification with TiO_2, both the shape and morphology of the TiO_2/SiO_2 composites, as captured by HR-TEM, were drastically altered. As shown in Figure 4, the large pores of *C. striata* biosilica were densely filled by TiO_2 nanoparticles of 10−40 nm in diameter. For the composite with the highest titania loading, the entire surface of biosilica appeared to be covered by nanoparticles (Figure 4a). The TiO_2 particles were likely to be deposited via physisorption as no change was observed in the FT-IR spectra (Figure 1b,c). Upon larger magnification of HR-TEM (scale of 10 nm), the crystalline lattices of the immobilized TiO_2 nanoparticles were visible (Figure 4b−d). Furthermore, the repeated black-white lines (Figure 4d) were indicative of highly structured channels within the crystal, in which each channel had a varying diameter in the range of 0.03−0.33 nm. As pure biosilica showed no structural organization at this magnification (Figure 3c), the lattice patterns clearly belonged to the immobilized TiO_2 nanoparticles. This prompted us to examine the particles using XRD and SAED (in conjunction with HR-TEM).

XRD analysis (Figure 5a) showed that the immobilized TiO_2 adopted an anatase phase at any ratio of Ti/Si (JCPDS-00-021-1272). Compared to the rutile phase, the anatase phase was suggested to be more photocatalytically active.[22] Furthermore, as confirmed by SAED analysis, while the initial biosilica was amorphous (Figure 5b), TiO_2/biosilica was polycrystalline (Figure 5c). Some observed rings in the SAED patterns of TiO_2/biosilica composite (Figure 5c) were well indexed with the characteristic planes of XRD results (JCPDS card No. 21-1272), namely, the 101 and 200 lattices. The 101 lattice has been reported as a stable anatase lattice for photocatalysis.[22]

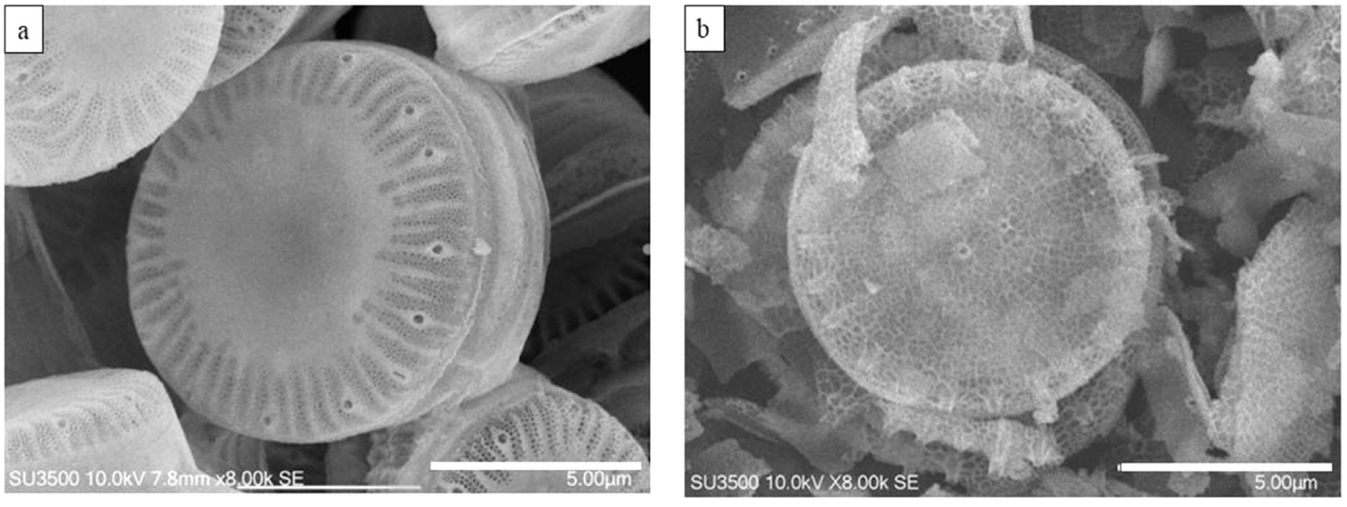

Figure 2. SEM images of (a) biosilica of *C. striata* diatom and (b) TiO_2-modified biosilica of *C. striata* diatom (scale of 5 μm).

https://doi.org/10.1021/acsomega.2c05450
ACS Omega 2022, 7, 44047−44056

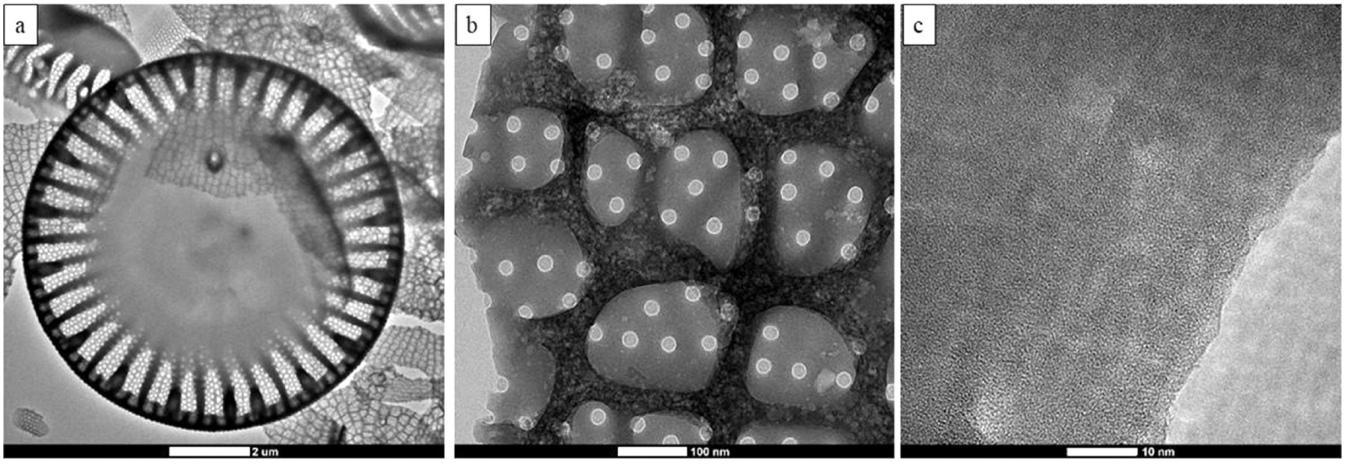

Figure 3. HR-TEM images of biosilica of *C. striata* diatom at different length scales: (a) scale of 2 μm, (b) scale of 100 nm, and (c) scale of 10 nm.

To determine the band gap, we recorded the light absorption of TiO_2 nanoparticles using UV−vis DRS (Figure 6a). TiO_2 possessed a band gap of 3.41 eV without any biosilica, which significantly decreased to around 3.2 eV upon deposition on the biosilica surface based on Tauc plots (Figure 6b). A lower band gap of the TiO_2/biosilica system indicates that less energy was required to excite an electron from the valence band to the conduction band. Therefore, a broad-range light source mimicking sunlight, such as a xenon lamp, could be used to trigger the catalysis. TiO_2/SiO_2 composites were then subjected to POME samples for photocatalytic investigation (Figures 7 and S4).

The photocatalytic activity of TiO_2/biosilica photocatalyst with different ratios was evaluated by degradation of POME waste under 300 W xenon lamp irradiation (UV−vis light, Figures 8 and S5). In addition, calibration of standard COD solutions (Figure S5) was conducted before assessing the performance of photocatalysts. The correlation between the degradation results and the reaction time for TiO_2/biosilica photocatalysts with different ratios is shown in Figure 8a, indicating that the degradation efficiency followed a hyperbolic trend. This may indicate that photocatalyst deactivation has occurred, most likely through the adsorption of intermediate organic species at the active sites. Consequently, the number of active sites decreases with irradiation time. Nevertheless, the photocatalyst with the highest titania content achieved the most effective POME degradation, reaching a 47% decrease in COD (Figure 8a) or twofold higher than the control (*i.e.*, neat TiO_2 catalyst). The exhibited efficiency (around 50%) was comparable to other photocatalytic systems tested for POME degradation (Table 2). Control experiments using *C. striata* biosilica (SiO_2) revealed negligible POME photodegradation in the absence of titania (Figure 8a).

A linear plot of $\ln(COD_0/COD)$ versus irradiation time t (min) for POME waste degradation is shown in Figure 8b, where the value of k is determined from the linear slope. The apparent reaction rate constant k was used to evaluate the degradation rate, as shown in Figure 8c. Photocatalysts with the highest TiO_2 loading exhibited the highest reaction rate constant. The value of R^2 obtained from 0.85 to 0.99 indicates very good linearity, which confirms that POME effluent degradation follows quasi-first-order reaction kinetics. Besides the highest titania content, the increased photocatalytic activity of the 54% TiO_2 photocatalyst could be attributed to the larger grain size, mesoporous structure, and lower specific surface area (as confirmed with BET isotherms analyses, Figure S3 and Table S2). Consequently, it can reduce the migration length of photogenerated charge carriers and the rate of photogenerated electron-hole pair recombination.

The photocatalytic degradation rates and reaction rate constants of the photocatalysts were found to decrease in the following order: 54% TiO_2 > 41% TiO_2 > 28% TiO_2 > 49% TiO_2 > 8.5% TiO_2. The presence of biosilica together with TiO_2 exhibit the rise of hydroxyl radical generation,[23,24] which is one of the main reactive oxygen species (ROS) in oxidizing POME waste. The hydroxyl radical $OH^{\bullet}$ is a powerful and nonselective oxidant (E° = +2.80 V) that causes partial or complete degradation of some organic chemicals.[25] It should be noted that the photocatalyst with 49% loading of TiO_2 originated from the highest initial concentration of Ti (75% Ti to 25% Si in mole ratio). At this initial ratio, the biosilica surface seemed to be already oversaturated with TiO_2 nanoparticles, and therefore additional TiO_2 might be prone to aggregation on the surface, hence lowering the photoactivity. Furthermore, photostability tests of the best-performing catalyst (53.79% TiO_2/SiO_2) were also examined throughout reaction cycles (Figure S6). These tests revealed only a small decrease in the reaction rate constant (k) over three reaction cycles (Figure 8d). The composite showed a loss of only 17% of photoactivity in the third run compared to the fresh sample, indicating that the physicochemical properties of the composite were preserved throughout the reaction cycles.

Based on the above findings, the proposed photocatalytic mechanism for POME degradation using TiO_2/biosilica composite is illustrated in Figure 9. First, light excitation on the photocatalyst generates photoexcited electrons (e_{CB}^-) and photogenerated holes (h_{VB}^+). Then, photogenerated holes can react spontaneously with water (H_2O) and hydroxyl group (OH^-) to produce hydroxyl radicals ($^{\bullet}OH$),[5,9,10,23−25] acting as an essential species in the degradation of POME waste. On the other hand, photoexcited electrons will be captured by the oxygen gas (O_2), which is adsorbed on the surface of the composite and produces superoxide radicals $^{\bullet}O_2^-$. The reactive oxygen species (superoxide and hydroxyl radicals)[26−33] oxidize the POME molecules adsorbed on the TiO_2/biosilica composites. Pollutant adsorption is likely to occur on the biosilica surface first and then transported to titania nanoparticles (situated on the pores and on the surface of the

https://doi.org/10.1021/acsomega.2c05450
ACS Omega 2022, 7, 44047−44056

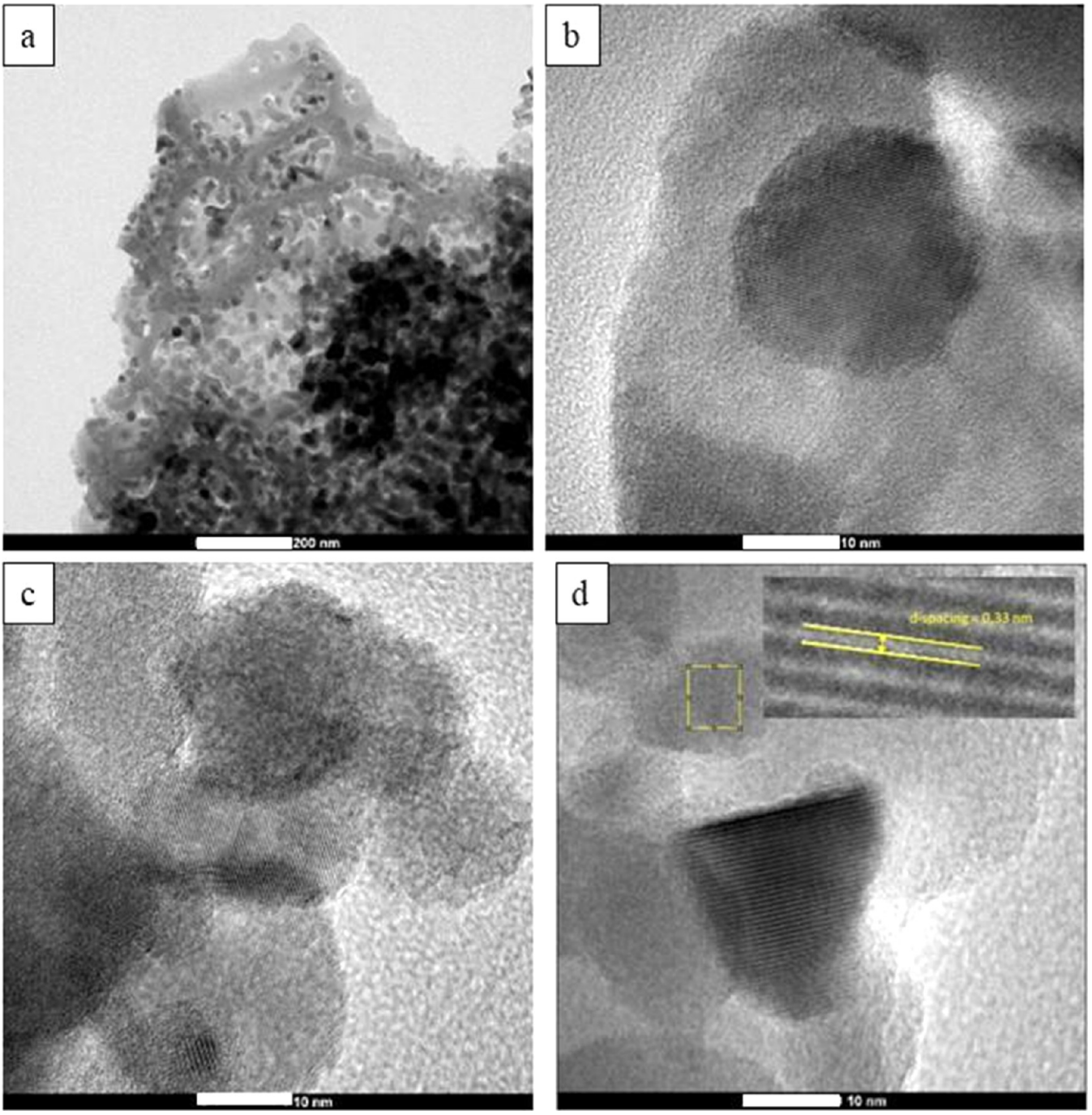

Figure 4. TEM images of the photocatalyst consisting of 54% TiO_2 at a scale of (a) 200 nm and (b)−(d) at 10 nm (taken for different particles in the vicinity). The inset in (d) shows the channel diameter in the lattice.

biosilica) as the active sites for photocatalytic degradation (*i.e.*, an adsorb-and-shuttle mode).[8,9] At last, these findings fill the gap in TiO_2-based photocatalyst applications for photocatalytic degradation of POME waste (Table 2).

On the other hand, the decrease in photocatalytic activity when increasing SiO_2 content can be ascribed to the less efficient separation of the photogenerated charge carriers and the decrease of quantum yield due to the higher band gap of SiO_2 (~11 eV). Moreover, based on XRD analysis (Figure 5), with an increasing amount of SiO_2 in the TiO_2/SiO_2 composite, the peak intensity of the anatase phase decreases, indicating that the TiO_2 exists mainly in the amorphous phase. In addition, the excess amount of SiO_2 in the composite may shield the TiO_2 photocatalysts, resulting in poor catalytic activity. It has been reported that amorphous TiO_2 has a lower photocatalytic activity compared to crystalline TiO_2.[23]

Nevertheless, the photocatalytic performance and reaction rate kinetics of 54% TiO_2/biosilica is still low compared to several other semiconductor-based photocatalysts (Table 2). Hence, further works could consider modifying some physicochemical properties of the TiO_2 photocatalyst and biosilica, including the density of active sites, band gap energy, specific surface area, phase composition, morphology, crystal facet engineering, etc. Future studies could also investigate the addition of metal and nonmetal dopants to generate solar-light-based photocatalysts for large-scale applications.

https://doi.org/10.1021/acsomega.2c05450
ACS Omega 2022, 7, 44047−44056

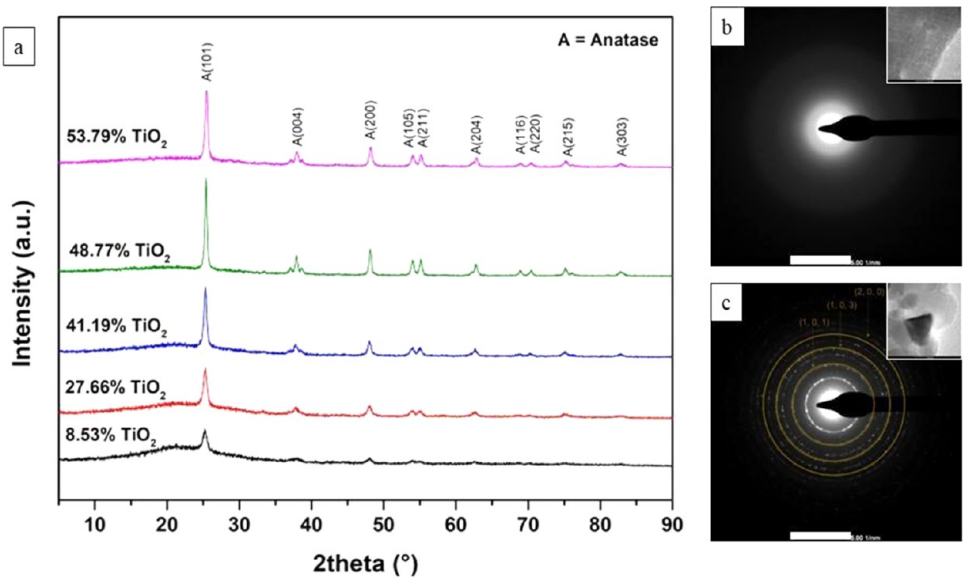

Figure 5. Examination of crystallinity based on (a) XRD spectra of photocatalysts at a varying ratio of Ti/Si, (b) SAED pattern of biosilica, and (c) SAED pattern of TiO_2-modified biosilica (54% TiO_2). Insets in (b) and (c) show the corresponding HR-TEM images of the selected areas.

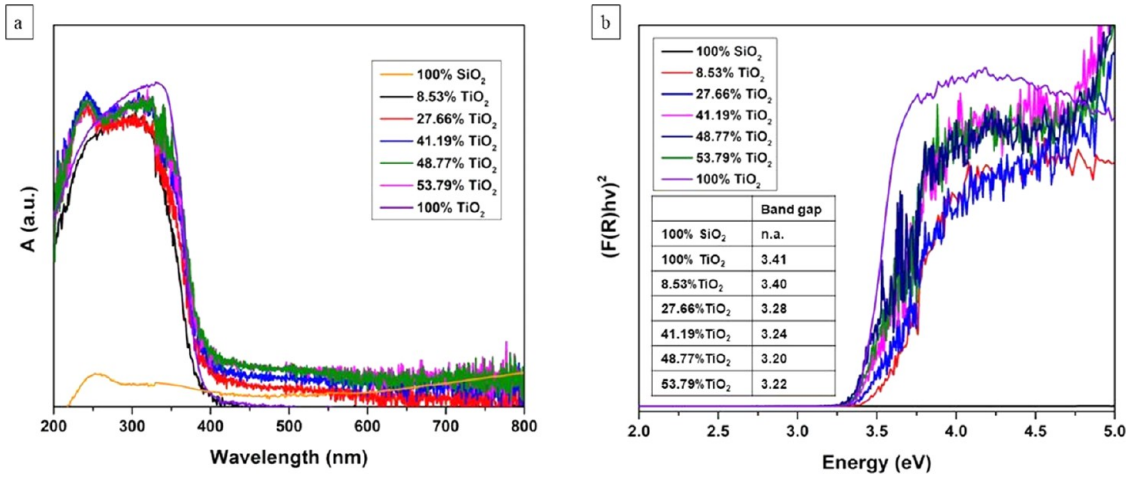

Figure 6. Absorbance and band gap analyses of biosilica (SiO_2), TiO_2, and TiO_2/SiO_2 with various ratios based on (a) UV−vis DRS spectra and (b) Tauc's plots.

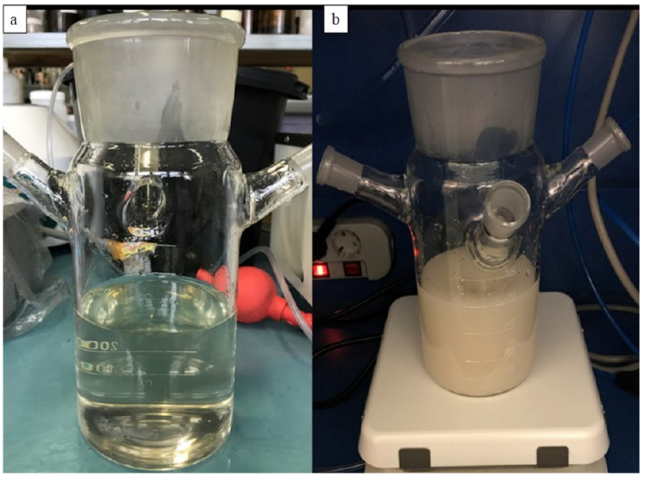

Figure 7. (a) Diluted POME waste and (b) suspension of POME waste and catalyst mixtures.

3. CONCLUSIONS

We have reported the structural characterization and evaluation of photoactivity of TiO_2/biosilica photocatalysts for POME degradation using live cultures of *C. striata* TBI strain as the starting materials. Upon reaching a maximum of 54% titania loading, we observed that the photocatalysts displayed significant POME degradation that followed a hyperbolic trend and exhibited good photostability over three reaction cycles. Through extensive imaging and physicochemical characterizations, we suggested that TiO_2 nanoparticles were trapped in a catalytically active anatase phase as polycrystalline particles with distinct lattices. The nature of the immobilization of TiO_2 on the biosilica surface was likely to be physisorption, as no change was indicated in the FT-IR spectra. Such entrapment has led to a decrease in the band gap of TiO_2 to around 3.2 eV, as opposed to 3.41 eV for bulk TiO_2 starting materials. Notably, photocatalytic degradation of POME using a wide-range xenon lamp was successfully performed (up to 47% POME degradation), which followed quasi-first-order kinetics. Thus, modified TiO_2/biosilica from diatoms can be used for POME

https://doi.org/10.1021/acsomega.2c05450
ACS Omega 2022, 7, 44047−44056

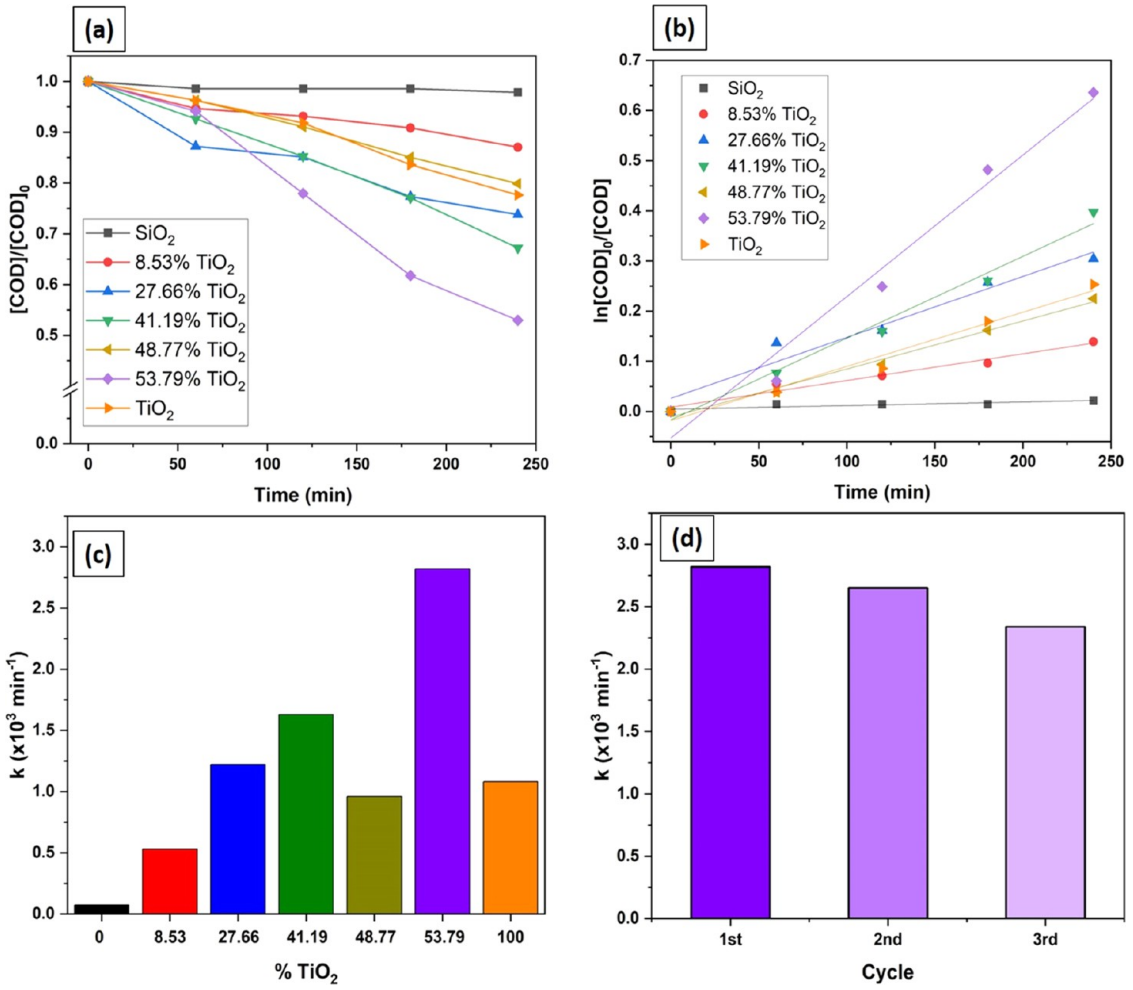

Figure 8. (a) Photocatalytic degradation of POME (b) Pseudo-first-order linear plots of $\ln(COD_0/COD)$ versus irradiation time for the degradation kinetics of POME using TiO_2/SiO_2 photocatalysts with varying TiO_2/SiO_2 ratios. (c) Apparent first-order rate constants (k) of TiO_2/SiO_2 composites with different TiO_2/SiO_2 ratios. (d) Comparison of the apparent first-order rate constant (k) of TiO_2/SiO_2 composites through a photocatalytic stability test over three reaction cycles for POME degradation using 53.79%TiO_2/SiO_2 catalyst.

Table 2. State of the Art for Photocatalytic Performance for POME Degradation Using Various Photocatalysts

photocatalyst	light source	catalyst loading (g/L)	initial COD (ppm)	photocatalytic performance	refs
TiO_2	UV fluorescent tube (20 W)	0.01	350	COD removal: 97% (42 min)k = n.a.	26
TiO_2	UV lamp (100 W)	1.0	~170	COD removal: 52% (4 h)$k = 2.90 \times 10^{-3}$ min^{-1}	27
TiO_2	UV lamp (100 W)	1.04	400	COD removal: 55% (4 h)k = n.a.	28
TiO_2 anatase	solar light	0.1	73 150	COD removal: 88% (5 h)k = n.a.	29
ZnO	mercury lamp (100 W)	1.0	~90	COD removal: 50% (4 h)$k = 3.12 \times 10^{-3}$ min^{-1}	30
ZnO-PEG	UV lamp (15 W)	0.5	n.a.	COD removal: 94% (30 min) k = n.a.	31
$CaFe_2O_4$	xenon lamp (500 W)	0.75	170−240	COD removal: 69% (8 h)$k = 2.71 \times 10^{-3}$ min^{-1}	32
$BiVO_4$	xenon lamp (300 W)	1.0	200−300	COD removal: 24% (4 h)$k = 1.04 \times 10^{-3}$ min^{-1}	33
54%TiO_2/biosilica	xenon lamp (300 W)	1.0	200−250	COD removal: 47% (4 h)$k = 2.82 \times 10^{-3}$ min^{-1}	this work

photodegradation and serve as an example of sustainable marine products for environmental remediation.

4. METHODS

The cultivation of *C. striata* was performed at a smaller scale of 1 L growth medium and then was adapted into larger-scale aquariums of 20 L growth medium containing modified seawater. The seawater consisted of various salts and carbon, nitrogen, and silica sources to grow the microalgae. The growth media were subjected to aeration using an air pump and controlled lightning using an LED (Krisbow lamp) with a photoperiodicity of 12:12 (h) on/off duration to allow photosynthesis. As indicated by the cell growth (Figure S1), after two weeks, the wet biomass was collected using centrifugation and electroflotation devices. The biomass of *C. striata* was then soaked in nitric acid for 45 min and repeated several times until the color of the biomass became yellowish white instead of the initial darker brown (Figure S2). Afterward, the treated biomass was rinsed with water until the pH reached 5. To obtain pure biosilica, the treated biomass was dried in an oven at 90 °C overnight and subsequently calcined at 550 °C for 10 h.[20] The biosilica was characterized using FT-IR (Prestige 21

https://doi.org/10.1021/acsomega.2c05450
ACS Omega 2022, 7, 44047−44056

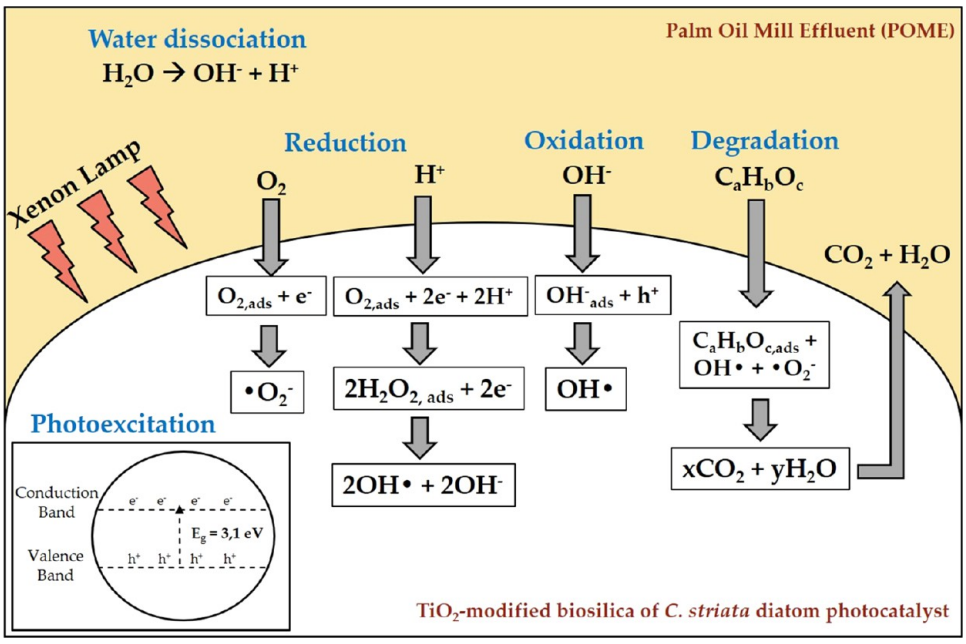

Figure 9. Proposed mechanism of POME photodegradation using biosilica/titania photocatalysts (Adapted with permission from Saputera et al.[33] Copyright 2021 by MDPI).

Shimadzu), XRF (EDAX Orbis), XRD (Bruker D8 Advance), SEM-EDX (Hitachi SU3500), and HR-TEM (FEI Tecnai G2 SuperTwin TEM/STEM) to obtain all information regarding chemical content, purity, and topology, respectively. Afterward, the biosilica was functionalized with titanium oxide using the precursor of titanium(IV) oxysulfate dissolved in water at 65 °C. The biosilica was added to the solution when it cooled down to room temperature and then stirred at 500 rpm for 2 h. Finally, the mixture was heated to 55 °C, and the resulting powder was calcined at 550 °C for 3 h.[6] The characterization of titanium oxide-modified biosilica was also performed using surface analysis (BET Quantachrome), FT-IR, XRF, XRD, diffuse reflectance UV−vis (8453 UV−vis spectrophotometer), HR-TEM, SAED, EDX, and SEM.

For the photocatalytic study, fresh POME was collected from the PTPN VII Palm Oil Mill in Bogor, Indonesia. For the study of POME photocatalytic degradation, fresh POME was filtered to remove the solid suspension, then diluted with deionized water. Filtration and dilution steps were required to ensure the light source could penetrate the reaction medium and activate the photocatalyst. Samples were evaluated through POME degradation under the UV−visible spectrum range. A photocatalyst of 0.5 g was added to 500 mL of pretreated POME (COD levels ranged from 200 to 250 mg/L) and stirred in the dark for 30 min until adsorption−desorption equilibrium was reached. At the same time, O_2 gas is introduced into the POME wastewater at a flow rate of 70−80 mL/min to provide a source of O_2 (Figure S4). The suspension is then irradiated using a 300 W xenon lamp (Toption Instrument Co., Ltd.) and mounted into a cooling water compartmen, which is circulated externally with water to remove heat lost from the light source (Figure S4). At irradiation intervals, every 60 min, 10 mL of the suspension was taken and filtered to remove photocatalyst particles using a syringe fitted with a 0.22 m nylon filter syringe. Each photocatalytic reaction was carried out for 240 min, and the POME concentration profile was obtained from COD analysis using a Hach DRB-200 COD reactor coupled with a UV−vis spectrophotometer (Shimadzu 1800 spectrophotometer). Calibration of the standard COD solution was conducted prior to evaluating the performance of photocatalysts (Figure S5a). The UV−vis absorbance spectra (with the wavelength interval of 550−650 nm) of the 53.79% TiO_2/SiO_2 composite for photocatalytic POME degradation are shown in Figure S5b.

The degradation efficiency, X (%), of the process is calculated using the following equation

$$\%X = \left(1 - \frac{C}{C_0}\right) \times 100$$

where C_0 is the initial COD value and C is the COD value at the time, t.

The reaction rate constant was then determined assuming quasi-first-order kinetics using the following equation

$$\ln\left(\frac{C_0}{C}\right) = kt$$

where C_0 is the initial COD concentration of POME waste (mg/L), C is the COD concentration of POME waste at time t (mg/L), and k is the reaction rate constant (1/min).

Catalyst stability was evaluated as follows: a catalyst composite was filtered after use, washed several times with distilled water, and finally dried at 100 °C for 24 h in static air. Resuspension in fresh POME waste solution was followed by the steps indicated above for fresh catalyst samples. Catalysts were used up to as much as three times.

■ ASSOCIATED CONTENT

Supporting Information

The Supporting Information is available free of charge at https://pubs.acs.org/doi/10.1021/acsomega.2c05450.

Growth curve of *Cyclotella striata* diatom, images and characterization of biomass and pure biosilica, BET isotherms for surface area analyses, photocatalytic reactor for POME degradation, calibration curve and UV−visible spectra of the 53.79% TiO_2/SiO_2 composite for POME

https://doi.org/10.1021/acsomega.2c05450
ACS Omega 2022, 7, 44047−44056

photodegradation, and photocatalytic stability test of the 53.79% TiO_2/SiO_2 composite for POME photodegradation (PDF)

AUTHOR INFORMATION

Corresponding Authors

Rindia M. Putri − *Biochemistry Division, Faculty of Mathematics and Natural Sciences, Institut Teknologi Bandung, Bandung 40132, Indonesia;* orcid.org/0000-0002-2264-4988; Email: rindia.m.putri@itb.ac.id

Wibawa Hendra Saputera − *Research Group on Energy and Chemical Engineering Processing System, Faculty of Industrial Technology, Institut Teknologi Bandung, Bandung 40132, Indonesia*; Email: hendra@che.itb.ac.id

Authors

Novi Syahra Almunadya − *Biochemistry Division, Faculty of Mathematics and Natural Sciences, Institut Teknologi Bandung, Bandung 40132, Indonesia*

Aryan Fathoni Amri − *Research Group on Energy and Chemical Engineering Processing System, Faculty of Industrial Technology, Institut Teknologi Bandung, Bandung 40132, Indonesia*

Nadia Tuada Afnan − *Biochemistry Division, Faculty of Mathematics and Natural Sciences, Institut Teknologi Bandung, Bandung 40132, Indonesia*

Zeily Nurachman − *Biochemistry Division, Faculty of Mathematics and Natural Sciences, Institut Teknologi Bandung, Bandung 40132, Indonesia*

Hary Devianto − *Research Group on Energy and Chemical Engineering Processing System, Faculty of Industrial Technology, Institut Teknologi Bandung, Bandung 40132, Indonesia*

Complete contact information is available at: https://pubs.acs.org/10.1021/acsomega.2c05450

Author Contributions

R.M.P.: conceptualization, funding acquisition, writing—original draft, methodology, and validation. N.S.A.: investigation, formal analysis, and methodology. A.F.A.: investigation and formal analysis. N.T.A.: formal analysis and visualization. Z.N.: resources and funding acquisition. H.D.: resources and funding acquisition. W.H.S.: conceptualization, funding acquisition, methodology, and writing—review and editing.

Notes

The authors declare no competing financial interest.

ACKNOWLEDGMENTS

This research is supported in part by The Asahi Glass Foundation Overseas Research Grant 2021 (Grant No. 1B/IT1.C02/TA.00/2021 to R.M.P.), the Institut Teknologi Bandung Research Grant 2021 (Grant No. 73/IT1.C02/TA.00/2021 to R.M.P.), and the Indonesian Ministry of Education, Culture, Research, and Technology Research Program 2022 (Grant No. 007/E5/PG.02.00.PT/2022 to Z.N. and Grant No. 007/E5/PG.02.00.PT/2022 to H.D. and W.H.S.). The authors thank Dr. Yanti Rachmayanti and team (Institut Teknologi Bandung) for sampling and genetic characterization of *C. striata* TBI strain. The authors acknowledge The Research Center of Nanoscience and Nanotechnology of Institut Teknologi Bandung (for XRF, XRD, and SEM-EDX measurements) and The Integrated Laboratory and Research Center of Universitas Indonesia (for HR-TEM and SAED measurements).

REFERENCES

(1) Sprintall, J.; Gordon, A. L.; Koch-Larrouy, A.; Lee, T.; Potemra, J. T.; Pujiana, K.; Wijffels, S. E. The Indonesian Seas and Their Role in the Coupled Ocean−Climate System. *Nat. Geosci.* **2014**, *7*, 487−492.

(2) Losic, D.; Rosengarten, G.; Mitchell, J. G.; Voelcker, N. H. Pore Architecture of Diatom Frustules: Potential Nanostructured Membranes for Molecular and Particle Separations. *J. Nanosci. Nanotechnol.* **2006**, *6*, 982−989.

(3) Bozarth, A.; Maier, U. G.; Zauner, S. Diatoms in Biotechnology: Modern Tools and Applications. *Appl. Microbiol. Biotechnol.* **2009**, *82*, 195−201.

(4) He, J.; Chen, D.; Li, Y.; Shao, J.; Xie, J.; Sun, Y.; Yan, Z.; Wang, J. Diatom-Templated TiO_2 with Enhanced Photocatalytic Activity: Biomimetics of Photonic Crystals. *Appl. Phys. A Mater. Sci. Process.* **2013**, *113*, 327−332.

(5) Sprynskyy, M.; Szczyglewska, P.; Wojtczak, I.; Nowak, I.; Witkowski, A.; Buszewski, B.; Feliczak-Guzik, A. Diatom Biosilica Doped with Palladium(II) Chloride Nanoparticles as New Efficient Photocatalysts for Methyl Orange Degradation. *Int. J. Mol. Sci.* **2021**, *22*, 6734.

(6) Ouwehand, J.; Van Eynde, E.; De Canck, E.; Lenaerts, S.; Verberckmoes, A.; Van Der Voort, P. Titania-Functionalized Diatom Frustules as Photocatalyst for Indoor Air Purification. *Appl. Catal. B Environ.* **2018**, *226*, 303−310.

(7) Mao, L.; Liu, J.; Zhu, S.; Zhang, D.; Chen, Z.; Chen, C. Sonochemical Fabrication of Mesoporous TiO_2 inside Diatom Frustules for Photocatalyst. *Ultrason. Sonochem.* **2014**, *21*, 527−534.

(8) Van Eynde, E.; Hu, Z. Y.; Tytgat, T.; Verbruggen, S. W.; Watté, J.; Van Tendeloo, G.; Van Driessche, I.; Blust, R.; Lenaerts, S. Diatom Silica-Titania Photocatalysts for Air Purification by Bio-Accumulation of Different Titanium Sources. *Environ. Sci. Nano* **2016**, *3*, 1052−1061.

(9) Van Eynde, E.; Tytgat, T.; Smits, M.; Verbruggen, S. W.; Hauchecorne, B.; Lenaerts, S. Biotemplated Diatom Silica-Titania Materials for Air Purification. *Photochem. Photobiol. Sci.* **2013**, *12*, 690−695.

(10) Gao, X.; Wachs, I. E. Titania−Silica as Catalysts: Molecular Structural Characteristics and Physico-Chemical Properties. *Catal. Today* **1999**, *51*, 233−254.

(11) Besançon, M.; Michelin, L.; Josien, L.; Vidal, L.; Assaker, K.; Bonne, M.; Lebeau, B.; Blin, J.-L. Influence of the Porous Texture of SBA-15 Mesoporous Silica on the Anatase Formation in TiO_2−SiO_2 Nanocomposites. *New J. Chem.* **2016**, *40*, 4386−4397.

(12) Urkasame, K.; Yoshida, S.; Takanohashi, T.; Iwamura, S.; Ogino, I.; Mukai, S. R. Development of TiO_2/SiO_2 Photocatalysts Having a Microhoneycomb Structure by the Ice Templating Method. *ACS Omega* **2018**, *3*, 14274−14279.

(13) Chetia, L.; Kalita, D.; Ahmed, G. A. Enhanced Photocatalytic Degradation by Diatom Templated Mixed Phase Titania Nanostructure. *J. Photochem. Photobiol. A Chem.* **2017**, *338*, 134−145.

(14) Gannavarapu, K. P.; Thakkar, M.; Veerapaga, S.; Wei, L.; Dandamudi, R. B.; Mitra, S. Novel Diatom-FeOx Composite as Highly Active Catalyst in Photodegradation of Rhodamine-6G. *Nanotechnol. Rev.* **2018**, *7*, 247−255.

(15) Padmanabhan, S. K.; Pal, S.; Ul Haq, E.; Licciulli, A. Nanocrystalline TiO_2/Diatomite Composite Catalysts: Effect of Crystallization on the Photocatalytic Degradation of Rhodamine B. *Appl. Catal. A Gen.* **2014**, *485*, 157−162.

(16) Gholami, P.; Khataee, A.; Bhatnagar, A. Photocatalytic Degradation of Antibiotic and Hydrogen Production Using Diatom-Templated 3D WO_3-X@mesoporous Carbon Nanohybrid under Visible Light Irradiation. *J. Clean. Prod.* **2020**, *275*, No. 124157.

(17) Saputera, W. H.; Amri, A. F.; Daiyan, R.; Sasongko, D. Photocatalytic Technology for Palm Oil Mill Effluent (POME). *Materials* **2021**, *14*, 2846.

https://doi.org/10.1021/acsomega.2c05450
ACS Omega 2022, 7, 44047−44056

(18) Herth, W. The Site of β-Chitin Fibril Formation in Centric Diatoms. II. The Chitin-Forming Cytoplasmic Structures. *J. Ultrastruct. Res.* **1979**, *68*, 16−27.
(19) Gale, D. K.; Gutu, T.; Jiao, J.; Chang, C.-H.; Rorrer, G. L. Photoluminescence Detection of Biomolecules by Antibody-Functionalized Diatom Biosilica. *Adv. Funct. Mater.* **2009**, *19*, 926−933.
(20) Jiang, W.; Luo, S.; Liu, P.; Deng, X.; Jing, Y.; Bai, C.; Li, J. Purification of Biosilica from Living Diatoms by a Two-Step Acid Cleaning and Baking Method. *J. Appl. Phycol.* **2014**, *26*, 1511−1518.
(21) Jeffryes, C.; Gutu, T.; Jiao, J.; Rorrer, G. L. Metabolic Insertion of Nanostructured TiO_2 into the Patterned Biosilica of the Diatom Pinnularia Sp. by a Two-Stage Bioreactor Cultivation Process. *ACS Nano* **2008**, *2*, 2103−2112.
(22) Luttrell, T.; Halpegamage, S.; Tao, J.; Kramer, A.; Sutter, E.; Batzill, M. Why Is Anatase a Better Photocatalyst than Rutile? - Model Studies on Epitaxial TiO_2 Films. *Sci. Rep.* **2015**, *4*, 4043.
(23) Xie, T.-H.; Lin, J. Origin of Photocatalytic Deactivation of TiO_2 Film Coated on Ceramic Substrate. *J. Phys. Chem. C* **2007**, *111*, 9968−9974.
(24) Narayanasamy, J.; Kubicki, J. D. Mechanism of Hydroxyl Radical Generation from a Silica Surface: Molecular Orbital Calculations. *J. Phys. Chem. B* **2005**, *109*, 21796−21807.
(25) Gligorovski, S.; Strekowski, R.; Barbati, S.; Vione, D. Environmental Implications of Hydroxyl Radicals (•OH). *Chem. Rev.* **2015**, *115*, 13051−13092.
(26) Haji Alhaji, M.; Sanaullah, K.; Fong Lim, S.; Ragai Henry Rigit, A.; Hamza, A.; Khan, A. Modeling and Optimization of Photocatalytic Treatment of Pre-Treated Palm Oil Mill Effluent (POME) in a UV/TiO_2 System Using Response Surface Methodology (RSM). *Cogent Eng.* **2017**, *4*, 1382980.
(27) Ng, K. H.; Cheng, C. K. A Novel Photomineralization of POME over UV-Responsive TiO_2 Photocatalyst: Kinetics of POME Degradation and Gaseous Product Formations. *RSC Adv.* **2015**, *5*, 53100−53110.
(28) Ng, K. H.; Cheng, C. K. Photocatalytic Degradation of Palm Oil Mill Effluent over Ultraviolet-Responsive Titania: Successive Assessments of Significance Factors and Process Optimization. *J. Clean. Prod.* **2017**, *142*, 2073−2083.
(29) Kanakaraju, D.; Ahmad, N. L. B.; Sedik, N. B. M.; Long, S. G. H.; Guan, T. M.; Chin, L. Y. Performance of Solar Photocatalysis and Photo-Fenton Degradation of Palm Oil Mill Effluent. *Malaysian J. Anal. Sci.* **2017**, *21*, 996−1007.
(30) Ng, K. H.; Cheng, C. K. Photo-Polishing of POME into CH_4-Lean Biogas over the UV-Responsive ZnO Photocatalyst. *Chem. Eng. J.* **2016**, *300*, 127−138.
(31) Zainuri, N. Z.; Hairom, N. H. H.; Sidik, D. A. B.; Desa, A. L.; Misdan, N.; Yusof, N.; Mohammad, A. W. Palm Oil Mill Secondary Effluent (POMSE) Treatment via Photocatalysis Process in Presence of ZnO-PEG Nanoparticles. *J. Water Process Eng.* **2018**, *26*, 10−16.
(32) Charles, A.; Khan, M. R.; Ng, K. H.; Wu, T. Y.; Lim, J. W.; Wongsakulphasatch, S.; Witoon, T.; Cheng, C. K. Facile Synthesis of $CaFe_2O_4$ for Visible Light Driven Treatment of Polluting Palm Oil Mill Effluent: Photokinetic and Scavenging Study. *Sci. Total Environ.* **2019**, *661*, 522−530.
(33) Saputera, W. H.; Amri, A. F.; Mukti, R. R.; Suendo, V.; Devianto, H.; Sasongko, D. Photocatalytic Degradation of Palm Oil Mill Effluent (POME) Waste Using $BiVO_4$ Based Catalysts. *Molecules* **2021**, *26*, 6225.

https://doi.org/10.1021/acsomega.2c05450
ACS Omega 2022, 7, 44047−44056